

# Echo-enhanced molecular orientation at high temperatures

Ilya Tutunnikov,<sup>1,\*</sup> Long Xu,<sup>1,\*</sup> Yehiam Prior,<sup>1,†</sup> and Ilya Sh. Averbukh<sup>1,‡</sup>

<sup>1</sup>*AMOS and Department of Chemical and Biological Physics,  
The Weizmann Institute of Science, Rehovot 7610001, Israel*

(Dated: July 19, 2022)

Ultrashort laser pulses are widely used for transient field-free molecular orientation – a phenomenon important in chemical reaction dynamics, ultrafast molecular imaging, high harmonics generation, and attosecond science. However, significant molecular orientation usually requires rotationally cold molecules, like in rarified molecular beams, because chaotic thermal motion is detrimental to the orientation process. Here we propose to use the mechanism of the echo phenomenon previously observed in hadron accelerators, free-electron lasers, and laser-excited molecules to overcome the destructive thermal effects and achieve efficient field-free molecular orientation at high temperatures. In our scheme, a linearly polarized short laser pulse transforms a broad thermal distribution in the molecular rotational phase space into many separated narrow filaments due to the nonlinear phase mixing during the post-pulse free evolution. Molecular subgroups belonging to individual filaments have much-reduced dispersion of angular velocities. They are rotationally cold, and a subsequent moderate terahertz (THz) pulse can easily orient them. The overall enhanced orientation of the molecular gas is achieved with some delay, in the course of the echo process combining the contributions of different filaments. Our results demonstrate that the echo-enhanced orientation is an order of magnitude higher than that of the THz pulse alone. The mechanism is robust – it applies to different types of molecules, and the degree of orientation is relatively insensitive to the temperature. The laser and THz pulses used in the scheme are readily available, allowing quick experimental demonstration and testing in various applications. Breaking the phase space to individual filaments to overcome hindering thermal conditions may find a wide range of applications beyond molecular orientation.

## I. INTRODUCTION

Control over the absolute orientation of molecules in space is essential for a wide variety of physical and chemical processes such as ultra-fast structural imaging, photon-induced processes, or chemical reactions [1–6]. Diverse optical methods have been developed to align and orient molecules in the gas phase under field-free conditions. A well-established route for orienting polar molecules is combining intense non-resonant laser fields with weak electrostatic fields [7–16]; another one involves using intense two-color laser pulses to induce molecular orientation via interaction with the molecular hyperpolarizability [17–31]. For chiral molecules, it is possible to induce orientation by using laser pulses with twisted polarization [32–38]. With the advance in terahertz (THz) technology, it has become possible to orient polar molecules using single- or half-cycle THz pulses through coupling to the permanent molecular dipole moment [39–49].

The efficiency of the above-mentioned methodologies deteriorates fast with increasing rotational temperature, and the molecular orientation is typically just a few percent at room temperature – too low for many practical applications. High temperature is detrimental to efficient orientation due to the increased dispersion of the molecular angular velocities with temperature. In laser-based methods, the degree of orientation may be enhanced by simply increasing the field intensity. Still, this approach has a practical limit because high-intensity laser pulses, especially two-color fields, give rise to significant molecular ionization, an undesired consequence of the strong field. On the other hand, in the case of THz pulses, the available field strengths are insufficient for achieving a sizable degree of orientation. Thus, attaining efficient molecular orientation at room temperatures is still an open, very challenging problem.

Over the years, several sophisticated proposals for enhancing molecular alignment and orientation have been put forward. These include applying optimized sequences of pulses [50–54], optimizing pulses’ parameters [55–64], and combining one-color laser pulses with two-color and THz pulses [65–74]. Several schemes were experimentally implemented [43, 75–77] and demonstrated improved orientation, mainly in the low-temperature regime.

Here, we propose an efficient and general approach for achieving significant field-free molecular orientation by moderate THz pulses even at room temperature. The method uses a pair of time-delayed pulses arranged in the echo configuration. The first, non-resonant laser pulse transforms a broad and smooth thermal probability-density distribution in the molecular rotational phase-space into multiple filaments (narrow strips). The second (typically weak) delayed THz excitation is then applied to the “filamented” molecular ensemble and causes a significant orientation of molecular groups belonging to different narrow filaments, each evolving independently. The enhanced ensemble-averaged orientation is achieved after some additional delay when the contributions of the independent filaments come together by the mechanism of echo formation. We show that for a proper choice of the excitation parameters, the amplitude of the orientation echo may be an order of magnitude higher than the orientation produced by the THz pulse alone. Moreover, the “filamenting” prepulse suppresses the detrimental effect of the molecular thermal rotational motion, making the echo amplitude rather insensitive to elevated temperatures.

Echoes are known in various domains of physics. The most notable example is Hahn’s spin-echo [78, 79] induced by two delayed magnetic field pulses. They result in a delayed magnetization response appearing after an additional delay equals the delay between the pulses. Various types of echoes have been discovered and studied in other fields, including photon echoes [80, 81], neutron spin-echo [82], cyclotron echoes [83], plasma-wave echoes [84], echoes in optically trapped cold atoms [85–87], echoes in particle accelerators [88–91], and echoes in free-electron lasers [92]. In addition, echoes in single quantum systems have been discussed [93, 94] and observed [95–97].

\* These authors contributed equally to this work

† [yehiam.prior@weizmann.ac.il](mailto:yehiam.prior@weizmann.ac.il)

‡ [ilya.averbukh@weizmann.ac.il](mailto:ilya.averbukh@weizmann.ac.il)

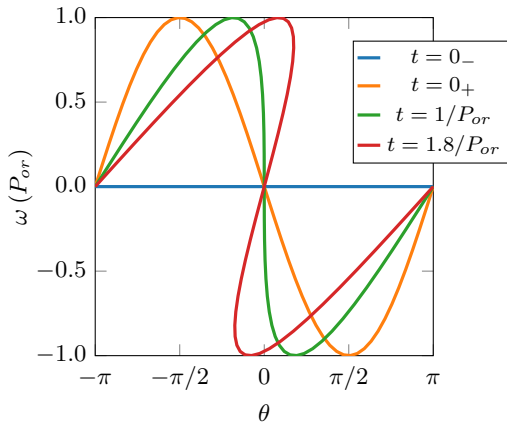


FIG. 1. Phase space following a single orienting kick at zero initial rotational temperature.

The enhancement mechanism of the present paper is related to the recently predicted and observed molecular alignment echoes [6, 98–108]. In contrast to the spin echoes [78, 79], they are based on the phenomenon of phase space filamentation known in non-linear systems, e.g., in the dynamics of stellar systems [109] and in accelerator physics [88, 90, 110]. Our paper presents the first application of the filamentation-based echoes to the problem of molecular orientation.

The paper is organized as follows. We begin with a qualitative physical description of the scheme using a simplified model of rigid planar rotors. Then we present the results of three-dimensional classical and fully quantum simulations of the echo-enhanced orientation of linear and symmetric-top molecules at room temperature. Finally, we summarize the results and discuss the prospects of the proposed scheme.

## II. QUALITATIVE DISCUSSION

To understand the physical principles behind the enhanced orientation, we start with a simplified planar rotor model, where a linear polar molecule is modeled as a rigid rotor restricted to rotate in the  $XY$  plane. To begin with, let us first consider the orientation dynamics induced by a single orienting kick. The orienting interaction potential is  $\propto -\cos(\theta)$ , where  $\theta$  is the angle between the molecular axis and the  $X$ -axis. Such a potential describes, e.g., the interaction of a single- or half-cycle THz pulse with the permanent molecular dipole.

*Single orienting kick* – In the impulsive approximation (when the change in  $\theta$  during the pulse is negligible),  $\theta$  and the molecule’s angular velocity,  $\omega$  after the orienting kick are given by

$$\theta(t) = \theta_0 + \omega t; \quad \omega = \omega_0 - P_{or} \sin(\theta_0), \quad (1)$$

where  $\theta_0$  and  $\omega_0$  are the initial angle and angular velocity.  $P_{or}$  is proportional to the amplitude of the orienting field,  $\varepsilon_{0,or}$  [for details, see Appendix A, Eq. (A5)] and has a physical meaning of the molecular angular velocity change due to the kick.

To study the rotational dynamics of an ideal molecular gas, we consider a collection of planar rotors that are initially isotropically distributed in the  $XY$  plane. At zero initial temperature, the phase space density before the

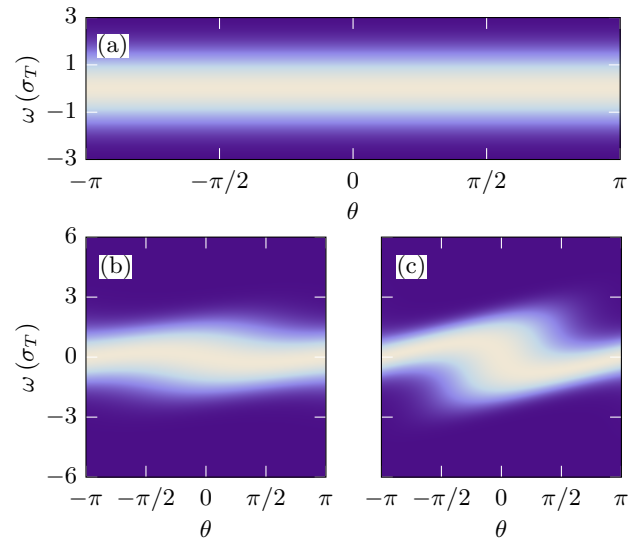


FIG. 2. Phase space distribution before and after a single orienting pulse. (a) At  $t = 0$ , before the kick. (b) After the pulse at  $t = \sigma_T^{-1}$  for a relatively weak orienting pulse  $P_{or} = 0.25\sigma_T$ . (c) After the pulse at  $t = \sigma_T^{-1}$  for a stronger orienting pulse  $P_{or} = 0.75\sigma_T$ .

kick is presented by a horizontal line  $\omega = 0$  (see Fig. 1,  $t = 0_-$ ). The orienting pulse transforms the initial distribution into a sine-shaped line ( $t = 0_+$ ). With time, the curve folds as particles with opposite angular velocities move in opposite directions along the  $\theta$  axis. The ensemble-averaged degree of orientation, or the orientation factor  $\langle \cos(\theta) \rangle$  reaches a universal maximum  $\approx 58\%$ , independent of  $P_{or}$  at  $t = 1.8/P_{or}$ .

At finite, non-zero initial rotational temperature, the initial phase space density is given by  $p(\theta, \omega, t = 0) = (2\pi)^{-3/2} \sigma_T^{-1} \exp[-\omega_0^2 / (2\sigma_T^2)]$ , see Fig. 2(a). The parameter  $\sigma_T = \sqrt{k_B T / I}$  defines the thermal dispersion of angular velocities, where  $T$  is the temperature,  $k_B$  is the Boltzmann constant and  $I$  is the moment of inertia of a single molecule. In the case of the initial thermal ensemble, the maximum degree of orientation is determined by the ratio  $P_{or} / \sigma_T \propto \varepsilon_{0,or} / \sqrt{T}$ . When the orienting kick is relatively strong (or, equivalently, the temperature is relatively low), the resulting orientation is high, and vice versa, when the kick strength is insufficient to overcome the thermal dispersion of angular velocities. The orientation factor after the kick is given by [for derivation, see Appendix B 1, Eq. (B5)]

$$\langle \cos(\theta) \rangle (t) = e^{-\sigma_T^2 t^2 / 2} J_1(P_{or} t), \quad (2)$$

where  $J_1(z)$  is the Bessel function of order one. When time is measured in units of  $1/\sigma_T$ , the orientation factor depends on the parameter  $P_{or} / \sigma_T$ . Unfortunately, the currently available THz pulses result in a weak deformation of the phase space density at room temperature. Shortly after a typical orienting kick, the phase space density is delocalized and looks like in Fig. 2(b). When the orienting kick is relatively strong (or, equivalently, the temperature is relatively low), the phase space distribution folds like in Fig. 2(c).

*Phase space filamentation* – To help a weak orienting pulse overcome the detrimental effect of high temperatures, we suggest stratifying the rotational phase space density into numerous separated strips (filaments). This way, the orienting pulse interacts with many individual

narrow filaments rather than a single broadly dispersed thermal distribution. For stratification, we use a relatively strong prepulse – a nonresonant linearly polarized short laser pulse that precedes the orienting one. Intense laser pulses interacting with molecular polarizability have been widely used for inducing transient field-free molecular alignment [1–5]. However, here we are not interested in the alignment effect but focus on the post-alignment stage characterized by highly stratified rotational phase space density [98, 100, 101] (see below).

A prepulse applied at  $t = 0$  transforms the rotors variables according to

$$\theta(t) = \theta_0 + \omega t; \quad \omega = \omega_0 - P_{pre} \sin(2\theta_0), \quad (3)$$

where  $P_{pre}$  is proportional to the intensity of the laser prepulse [for details, see Appendix A, Eq. (A9)]. The phase space density after the prepulse is described by

$$p(\theta, \omega, t) = \frac{\sigma_T^{-1}}{(2\pi)^{3/2}} \exp \left[ -\frac{(\omega + P_{pre} \sin[2\theta - 2\omega t])^2}{2\sigma_T^2} \right], \quad (4)$$

where we used Eq. (3) to express  $\omega_0$  in terms of  $\omega$  and  $\theta$  after the pulse, and substituted  $\omega_0$  into the Boltzmann distribution. The stratifying pulse imprints a sinusoidal shape on the phase-space density which folds with time. Shortly after the excitation, the phase-space distribution concentrates near  $\theta = 0, \pi$ , corresponding to alignment along the  $X$  axis [see Fig. 3(a)]. It's important for our discussion that with time, the phase space density undergoes filamentation and turns into a series of almost parallel filaments (strips) separated in angular velocity by  $\pi/t$  [see Eq. (4)]. Note that longer waiting times result in narrower filaments because the phase space volume is conserved.

After a delay  $\tau$  (at  $t = \tau$ ), when the filaments are numerous and thin, [see Fig. 3(b)], we apply the orienting THz kick. Now, each filament resembles the phase-space density of an isotropic cold molecular ensemble (see Fig. 1,  $t = 0_-$ ). Moreover, since the dispersion of angular velocities within each filament is much smaller than the initial thermal dispersion, the interaction with the weak orienting pulse results in non-negligible deformation of the filaments [see Fig. 3(c)].

With time, each filament folds like in Fig. 2(c) developing a bunch. This folding does not result in substantial orientation just after the orienting kick because the bunches move relative to each other (they are spaced apart by  $\pi/\tau$  along the  $\omega$  axis). Due to the “quasi-quantization” of the angular velocities, the folded filaments synchronize near  $\theta = 0, \pi$  after an additional time delay equal to  $\tau$  (at  $t \approx 2\tau$ , not shown). This synchronization manifests itself in alignment echo [6, 98–101, 107]. Similar synchronization dynamics is behind the echo phenomenon in several other nonlinear systems [88, 90, 93, 94, 97, 111].

After an additional delay of  $\tau$  (at  $t \approx 3\tau$ ), we witness another echo, and this is a new observation. The individual bunches re-synchronize in an asymmetric manner resulting in molecular orientation. First, the bunches accumulate near  $\theta = 0$  [just before  $t = 3\tau$ , see Fig. 3(d)], and then near  $\theta = \pi$  [just after  $t = 3\tau$ , not shown]. The closeups in Fig. 3(d) demonstrate that the bunches in each filament look similar to those seen in Fig. 2(c). Such re-synchronizations happen again at later times:  $t = 5\tau, 7\tau, \dots$ , and manifest themselves in orientation echoes of higher orders.

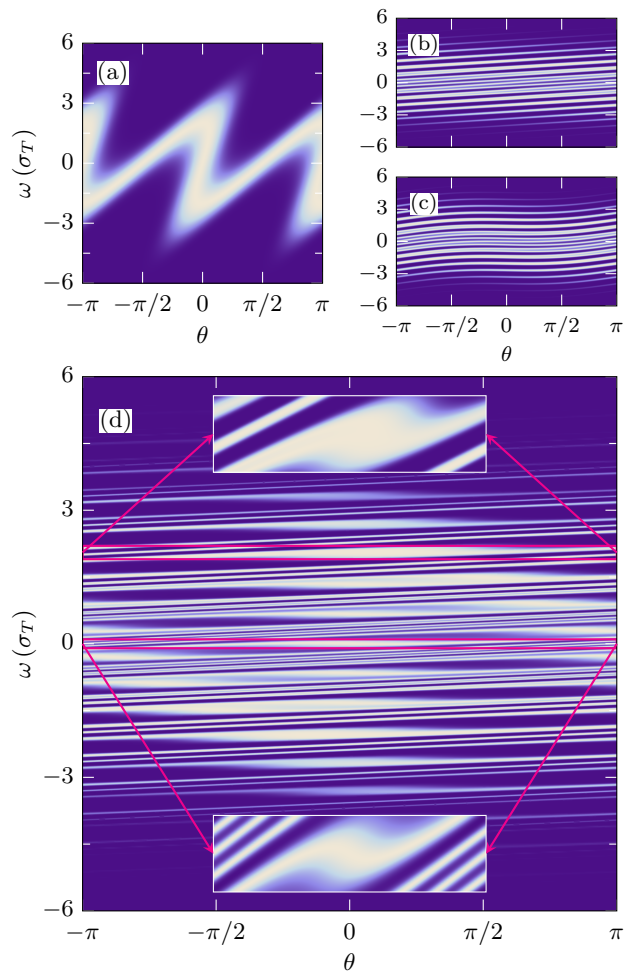


FIG. 3. Phase space distribution. (a) Shortly after the stratifying kick,  $t = 0.4/\sigma_T$ . (b) Just before the orienting kick,  $t = \tau_-$ , for  $\tau = 5/\sigma_T$ . (c) Just after the orienting kick,  $t = \tau_+$ . (d) Orientation along the  $X$  axis, before the time of the orientation echo at  $t = 3\tau$ . The regions marked in magenta are shown in the insets. Here  $P_{pre} = 2\sigma_T$ ,  $P_{or} = 0.25\sigma_T$ .

Figure 4 shows the time-dependent orientation factor,  $\langle \cos(\theta) \rangle$  for two delays,  $\tau = 10/\sigma_T$  and  $\tau = 20/\sigma_T$ . In both cases, the first orientation echo emerges after a delay equal to  $2\tau$ . However, compared to  $\tau = 10/\sigma_T$ , the echo amplitude for  $\tau = 20/\sigma_T$  is significantly higher. In line with the qualitative arguments presented above, longer delays give rise to thinner filaments which, in turn, “helps” the weak orienting kick.

The orientation factor in the presence of both stratifying and orienting kicks is given by [for derivation, see Appendix B 2, Eq. (B13)]

$$\langle \cos(\theta) \rangle (t) = \Theta(t - \tau) \sum_{\text{odd } k}^{\infty} S_k(t), \quad (5)$$

where  $\Theta(t - \tau)$  is the step-function and

$$S_k(t) = e^{-\sigma_T^2(t-k\tau)^2/2} J_k[P_{or}(t-\tau)] J_{\frac{k-1}{2}}[P_{pre}(k\tau-t)]. \quad (6)$$

The orientation signal consists of a series of pulsed responses separated in time by  $2\tau$ . The first orientation echo ( $k = 3$ ) is proportional to

$$S_3(t) \approx e^{-\sigma_T^2(t-3\tau)^2/2} J_3(2P_{or}\tau) J_1[P_{pre}(3\tau-t)]. \quad (7)$$

Here we used the facts that  $J_3(z)$  increases with  $z$  for  $z < 4$ , and  $t - 3\tau$  is relatively small (due to the Gaussian

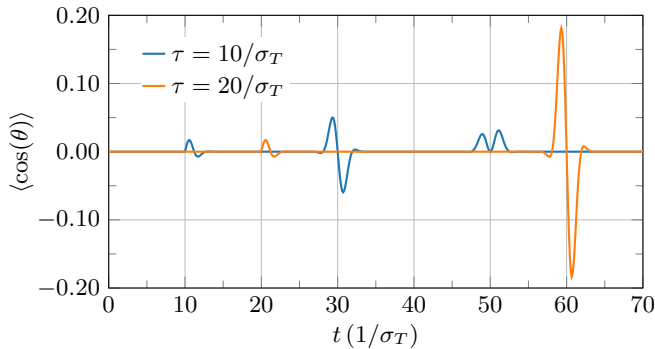


FIG. 4. Orientation factor following combined excitation by stratifying and orienting pulses. Here,  $P_{pre} = 2\sigma_T$ ,  $P_{or} = 0.1\sigma_T$ . Note the enhanced orientation at  $t = 2\tau$  for both cases of  $\tau = 10/\sigma_T$  and  $\tau = 20/\sigma_T$ , with the higher degree of orientation for the longer delay. With the orienting pulse alone, the maximal orientation factor is  $\approx 0.03$ .

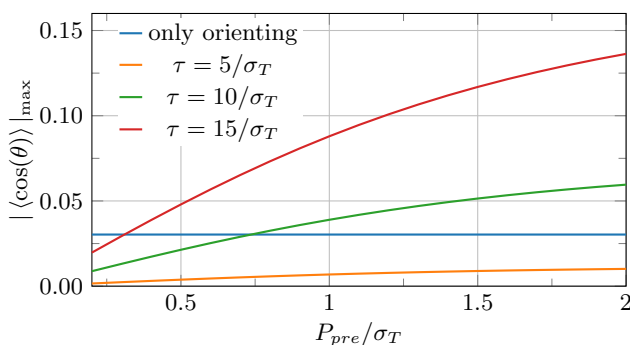


FIG. 5. Maximum orientation factor (absolute value) as a function of  $P_{pre}$  for fixed  $P_{or} = 0.1/\sigma_T$ . Note that for the low intensity prepulses, the degree of orientation is lower than in the absence of a prepulse altogether. This is a result of very minimal filamentation caused by the weak prepulses, which, in effect, slightly increases the dispersion of rotational velocities.

factor). This expression shows the essential feature of the proposed scheme – for fixed temperature and stratifying kick (prepulse) strength,  $\sigma_T$  and  $P_{pre}$ , the echo amplitude increases with  $P_{or}\tau$ . In other words, increasing the delay  $\tau$  is equivalent to increasing the orienting kick strength.

Moreover, the echo amplitude increases with  $P_{pre}$  as well. Figure 5 shows the maximum orientation factor for several delays as a function of  $P_{pre}$  (for fixed  $P_{or}$ ). When compared to the maximal orientation achieved by the orienting kick alone, the addition of the prepulse enhances the orientation starting from certain  $P_{pre}$  values (depending on the delay,  $\tau$ ). Note that if the prepulse is weak, it has a negative effect, namely the degree of orientation is even lower than when using only the orienting pulse. The reason is that a weak prepulse does not generate narrow well-separated filaments which can be distorted by the weak orienting pulse. Instead, it effectively slightly increases the dispersion of rotational velocities.

Terms with  $k > 3$  in Eq. (5) correspond to the orientation echoes of a higher order that typically (but not always) have lower amplitude compared to the first echo [6, 98–101, 111].

In the classical case, the delay  $\tau$  could, in principle, be increased indefinitely to achieve higher orientation. However, when the delay becomes comparable to the time of rotational quantum revivals [112, 113], the interplay be-

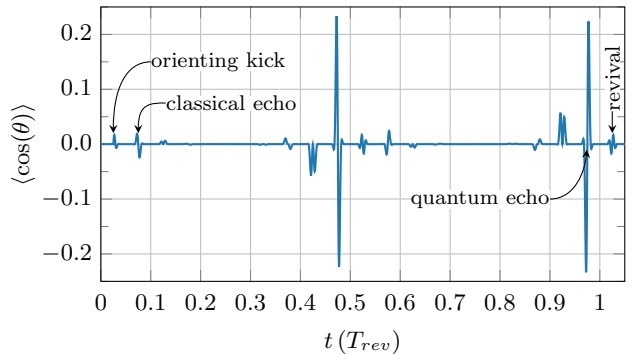


FIG. 6. Orientation factor calculated quantum mechanically at  $T = 300$  K. Here, the orienting kick is applied after a delay  $\tau = 0.025T_{rev}$ , which corresponds to  $\tau \approx 7.2/\sigma_T$ . The excitation strengths,  $P_{pre}$  and  $P_{or}$  are the same as in Fig. 4. When only the orienting pulse is applied, the maximal orientation is  $\approx 0.03$ .

tween echoes and revivals needs to be taken into account. As was shown previously [87, 93], a particular type of echo exists, termed *quantum echo*. A series of quantum echoes emerge on a long time scale just before the quantum revivals. These echoes have a valuable property – in the limit of weak echo-inducing excitation (the orienting kick in our case), their amplitude is higher than the classical echoes discussed. We take advantage of this to achieve even higher molecular orientation with constrained delays.

To illustrate this point, we consider the dynamics of a kicked quantum rigid 2D rotor (for details, see Appendix C). The rotational revival time of the quantum planar rotor is  $T_{rev} = 4\pi I/\hbar$ , where  $I$  is the moment of inertia. Figure 6 shows the orientation factor in the quantum model in the presence of the stratifying (prepulse) and orienting kicks. Here, for demonstration purposes, we choose a short time delay  $\tau = 0.025T_{rev}$  resulting in a relatively weak classical orientation echo at  $t = 3\tau = 0.075T_{rev}$ . The amplitude of the classical echo is comparable to the maximal orientation obtained when using the orienting pulse alone,  $\approx 3\%$ . In striking contrast, a quantum echo emerges at a delay  $-2\tau$  before the revival, at  $t = 0.975T_{rev}$  with a much higher amplitude of  $\approx 22\%$ . Notice that echoes of the same magnitude (but opposite sign) emerge just before the half revival. Alignment echoes emerging before the quantum revivals, the so-called imaginary echoes, were studied by us both theoretically and experimentally [100, 101].

### III. THREE-DIMENSIONAL SIMULATIONS

#### A. Numerical methods

So far, we considered the orientation enhancement in the simplified model of 2D rigid rotors. In this section, we apply the developed understanding to “real world” by considering the corresponding three-dimensional classical and quantum dynamics of linear and prolate symmetric-top molecules driven by the experimentally available laser and THz fields. The rotational dynamics is treated within the rigid rotor approximation. We model the time-dependent electric field, consisting of the delayed non-

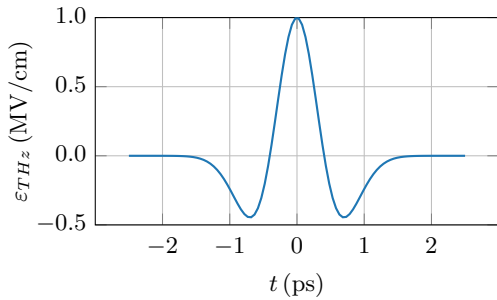


FIG. 7. Electric field of the THz pulse, given by  $\varepsilon_{THz}(t) = \varepsilon_{0,THz}(1 - 2\kappa t^2) \exp(-\kappa t^2)$ . Here,  $\varepsilon_{0,THz} = 1.0$  MV/cm,  $\kappa = 3.06$  ps $^{-2}$ .

resonant laser and single-cycle THz pulses, using

$$\mathbf{E}(t) = \varepsilon_{lsr}(t) \cos(\omega t) \mathbf{e}_Z + \varepsilon_{THz}(t - \tau) \mathbf{e}_Z, \quad (8)$$

where  $\omega$  is the carrier frequency of the laser pulse,  $\varepsilon_{lsr}(t) = \varepsilon_{0,lsr} \exp[-2 \ln 2 (t/\sigma_{lsr})^2]$ ,  $\varepsilon_{0,lsr}$  is the peak amplitude, and  $\sigma_{lsr}$  is the full width at half maximum (FWHM) of the laser pulse intensity profile.  $\varepsilon_{THz}(t) = \varepsilon_{0,THz}(1 - 2\kappa t^2) \exp(-\kappa t^2)$  [45, 46], where  $\varepsilon_{0,THz}$  is the peak amplitude of the THz pulse,  $\kappa$  determines the temporal width of the THz pulse.  $\tau$  is the time delay between the laser and THz pulses and  $\mathbf{e}_Z$  is a unit vector along the laboratory  $Z$  axis. Figure 7 shows the electric field amplitude of the THz pulse as a function of time.

*Classical simulation* – We use the Monte Carlo method to simulate the behavior of a classical ensemble. Initially,  $N = 10^7$  sample molecules are isotropically distributed in space. Their angular velocities are given by the Boltzmann distribution  $P(\Omega_i) \propto \exp[-I_i \Omega_i^2 / (2k_B T)]$ , where  $i = x, y, z$  refers to the molecular principal axes of inertia. In the case of a linear molecule  $I_z = 0$ ,  $I_x = I_y \equiv I$ , while in the case of a prolate symmetric-top molecule,  $I_z < I_x = I_y \equiv I$ . For each sample molecule, the rotational dynamics in the rotating molecular frame is described by Euler's equations [114]

$$\mathbf{I}\dot{\boldsymbol{\Omega}} = (\mathbf{I}\boldsymbol{\Omega}) \times \boldsymbol{\Omega} + \mathbf{T}, \quad (9)$$

where  $\mathbf{I} = \text{diag}(I_x, I_y, I_z)$  is the moment of inertia tensor,  $\boldsymbol{\Omega} = (\Omega_x, \Omega_y, \Omega_z)$  is the angular velocity, and  $\mathbf{T} = (T_x, T_y, T_z)$  is the torque due to the interactions with the external electric field. The laser field interacts with the molecular polarizability  $\boldsymbol{\alpha} = \text{diag}(\alpha_{xx}, \alpha_{yy}, \alpha_{zz})$ , and the torque is given by  $\mathbf{T} = [\boldsymbol{\alpha} \mathbf{E}_{mol}(t)] \times \mathbf{E}_{mol}(t)$ . The THz field interacts with the molecular permanent dipole moment,  $\boldsymbol{\mu}$ , and the torque is given by  $\mathbf{T} = \boldsymbol{\mu} \times \mathbf{E}_{mol}(t)$ . Here,  $\mathbf{E}_{mol}(t)$  is the representation of the electric field vector in the basis of the molecular principal axes. The relation between the laboratory and the rotating molecular frames is parametrized by a quaternion,  $q = (q_0, q_1, q_2, q_3)$  [115, 116]. The quaternion's equation of motion is  $\dot{q} = q\boldsymbol{\Omega}/2$ , where the quaternions multiplication rule is assumed, and  $\boldsymbol{\Omega} = (0, \Omega_x, \Omega_y, \Omega_z)$ . The orientation factor at time  $t$  is obtained by averaging over all sample molecules (ensemble average). A more detailed description of the classical simulations can be found in [31, 36].

*Quantum simulation* – The Hamiltonian describing the rotational dynamics in the presence of external fields [see Eq. (8)] is [5, 117]

$$H(t) = H_r - \boldsymbol{\mu} \varepsilon_{THz}(t) \cos(\theta) - \frac{\Delta\alpha}{4} \varepsilon_{lsr}^2(t) \cos^2(\theta), \quad (10)$$

where  $H_r$  is the rotational kinetic energy Hamiltonian,  $\boldsymbol{\mu} = |\boldsymbol{\mu}|$  is the permanent molecular dipole moment,  $\Delta\alpha = \alpha_{zz} - \alpha_{xx} = \alpha_{zz} - \alpha_{yy}$  is the polarizability anisotropy, and  $\theta$  is the polar angle between the molecular symmetry axis and the laboratory  $Z$  axis (field polarization axis). The polarizability interaction term is averaged over the optical cycle.

In the simulations, the wave function  $\Psi$  is expressed in the basis of the eigenfunctions of  $H_r$ . For a linear molecule, these are the spherical harmonics  $Y_J^M(\theta, \phi)$  ( $\phi$  is the azimuthal angle), while for a symmetric-top molecule, these are Wigner D-functions  $D_{MK}^J(\theta, \phi, \chi)$ , where  $\chi$  is the angle of rotation about the molecular symmetry axis. The quantum numbers  $J$ ,  $M$  and  $K$  correspond to the magnitude of the angular momentum, projection of angular momentum on the laboratory  $Z$  axis, and projection of the angular momentum on the molecular symmetry axis. The eigenenergies are  $E_J = BJ(J+1)$  (linear molecule) and  $E_{JK} = CJ(J+1) + (A-C)K^2$  (symmetric-top molecule), where  $B = C = \hbar^2/(2I)$  and  $A = \hbar^2/(2I_z)$ . The time-dependent Schrödinger equation is solved by numerical exponentiation of the Hamiltonian matrix (see Expokit [118]).

In the case of the linear molecule, the orientation factor is given by the averaged expectation value

$$\langle \cos(\theta) \rangle(t) = \frac{1}{Z} \sum_{JM} \langle \cos(\theta) \rangle_{JM}(t) e^{-E_J/(k_B T)}, \quad (11)$$

where  $Z$  is the partition sum,  $\langle \cos(\theta) \rangle_{JM}(t) = \langle \Psi_{JM}(t) | \cos(\theta) | \Psi_{JM}(t) \rangle$  for the initial state  $\Psi_{JM}(t=0) = Y_J^M$ , and the sum runs over all the thermally populated eigenstates  $Y_J^M$ .

In the case of symmetric-top molecules, due to the increased number of thermally populated states, we use the random phase wave functions method (see, e.g. [119]) to simulate the behavior of the thermal ensemble. The orientation factor is given by the average

$$\langle \cos(\theta) \rangle(t) = \frac{1}{N} \sum_{n=1}^N \langle \cos(\theta) \rangle_n(t), \quad (12)$$

where  $N$  is the number of initial states used,  $\langle \cos(\theta) \rangle_n(t)$  is the orientation factor obtained for the initial state  $\psi_n$

$$\psi_n = \sum_{JKM} \sqrt{\frac{\epsilon_K e^{-E_{JK}/(k_B T)}}{Z}} D_{MK}^J e^{i\varphi_{n,JKM}}, \quad (13)$$

where  $\varphi_{n,JKM} \in [0, 2\pi)$  is a random number and the sum runs over all the thermally populated eigenstates  $D_{MK}^J$ . For CH<sub>3</sub>I molecule, the statistical weight due to the nuclear spin statistics is given by [120]

$$\epsilon_K = \frac{(2I_H + 1)^3}{3} \left[ 1 + \frac{2 \cos(2\pi K/3)}{(2I_H + 1)^2} \right], \quad (14)$$

with  $I_H = 1/2$ .

## B. Results: linear molecule

We consider OCS as an example linear molecule. The molecular properties were taken from NIST (DFT, method: CAM-B3LYP/aug-cc-pVTZ) [121]:  $I = 83.021$  amu Å<sup>2</sup>,  $\boldsymbol{\mu} = 0.755$  Debye, and  $\Delta\alpha = 3.738$  Å<sup>3</sup>.

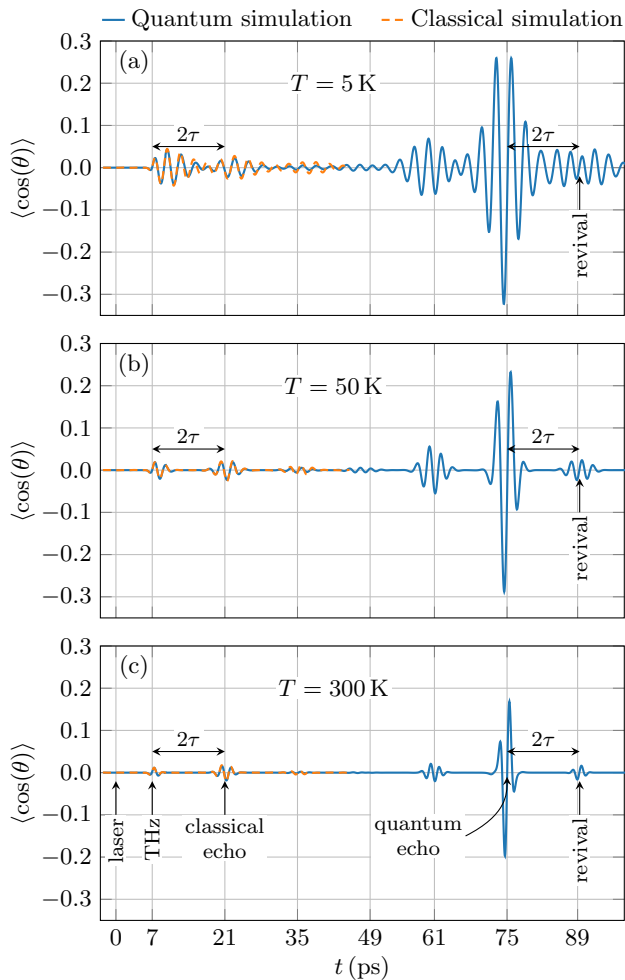


FIG. 8. Orientation factor for OCS molecules at different temperatures. The molecules undergo combined excitation by stratifying pulse followed by a THz pulse with a delay  $\tau = 7$  ps. The temperatures are: (a) 5 K, (b) 50 K, and (c) 300 K, and the maximum orientation factors obtained without the stratifying laser pulses are 0.0074, 0.0201, and 0.0215, respectively.

The rotational revival time of the OCS molecule is  $T_{rev} = 1/(2cB) \approx 82.4$  ps, where  $c$  is the speed of light.

Figure 8 shows the time-dependent orientation factor,  $\langle \cos(\theta) \rangle(t)$  obtained using classical and quantum simulations. The molecules were excited by the delayed laser and THz pulses [see Eq. (8)] at different initial rotational temperatures. The delay between the pulses was set to  $\tau = 7$  ps. The peak intensity of the laser pulse is  $I_{0,lsr} = 4 \times 10^{13}$  W/cm<sup>2</sup>, FWHM is  $\sigma_{lsr} = 100$  fs. The THz pulse parameters are  $\varepsilon_{0,THz} = 1.0$  MV/cm,  $\kappa = 3.06$  ps<sup>-2</sup>. Laser and THz pulses with similar parameters are readily available nowadays [122–125].

Both quantum and classical simulations demonstrate an immediate orientation response emerging during and shortly after the THz pulse excitation (at  $t \approx 7$  ps). The first classical echo appears with a delay  $2\tau$  after the THz pulse, at  $t \approx 21$  ps. The quantum mechanical result shows a strong echo signal before the orientation quantum revival, at  $t \approx 75.4$  ps. The magnitude of this echo is an order of magnitude larger than the maximum orientation induced by THz pulse alone. In agreement with the previous studies [87, 93] and the qualitative analysis based on the simplified models (see Sec. II), the orientation during the quantum echo is significantly higher compared to

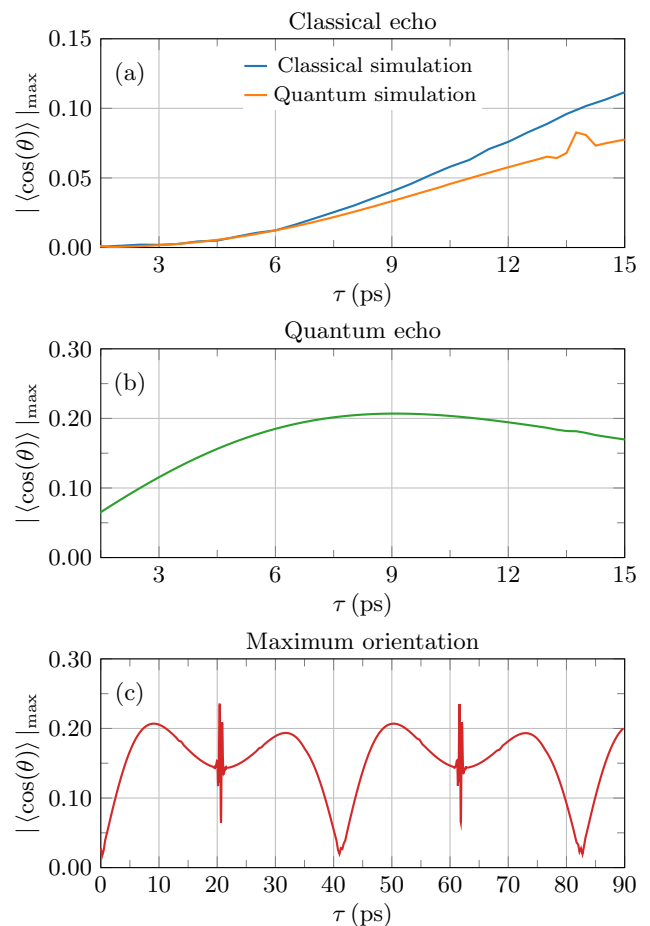


FIG. 9. Maximum orientation factor (OCS molecule,  $T = 300$  K, absolute value) as a function of  $\tau$  (the delay between the prepulse and the orienting THz pulse) in different time windows. (a) During the classical echo emerging after delay equal  $2\tau$  after the THz excitation,  $t \approx 3\tau$ . (b) During the quantum echo emerging at delay equal  $-2\tau$  before the orientation quantum revival,  $t \approx T_{rev} - \tau$ . (c) The global maximum of the orientation factor after the THz pulse. The field parameters are the same as in Fig. 8. For comparison, the maximum orientation factor without the stratifying pulse is  $\approx 0.0215$ .

the orientation during the classical echo. The magnitude of the quantum echo dominates at all temperatures represented in Fig. 8, including the room temperature, see Fig. 8(c).

Remarkably, the echo amplitude weakly depends on temperature (in the presented temperature range). This behavior can be understood with the help of the simplified model introduced in Sec. II. The laser pulse is intense enough to induce efficient phase-space filamentation at all the represented temperatures. With time, the number of filaments grows, and they become thinner. As a result, each molecular subgroup forming a single filament has much reduced dispersion of angular velocities (caused by chaotic thermal motion), and it is effectively “cold”. Instead of competing with the highly dispersed angular velocities of the initial thermal ensemble, the weak THz pulse competes against the cold narrow filaments. When the change  $P_{or}$  of the rotation velocity due to the orienting pulse exceeds the width of the cold filaments, the following orientation echo dynamics becomes insensitive to this width, and, hence, to the initial molecular temperature.

As noted in the caption of Fig. 8 with the actual THz

pulses used here, the dependence of the maximal orientation obtained using the THz pulse only is counterintuitive, namely, the maximal orientation factor slightly increases with temperature instead of decreasing. This is in contrast to the case of impulsive orienting kicks considered in Sec. II. For relatively long THz pulses, the frequency contents of the pulse match the transitions between higher rotational levels and therefore is more effective in orienting higher temperature ensembles. A similar non-trivial behavior was studied theoretically in [126]. The dependence of orientation echoes on the pulse duration and other parameters will be elaborated further in a forthcoming publication.

As discussed in Sec. II, the echo amplitude increases with the time delay between the stratifying and orienting pulses (for fixed temperature and field parameters). Figure 9 shows the maximum orientation during the first classical echo [at delay  $2\tau$  after the THz pulse, see panel (a)] and during the quantum echo [at delay  $-2\tau$  before the orientation revival, see panel (b)] for relatively short delays  $\tau$ . For  $\tau < 15$  ps, the magnitude of both types of orientation echoes increases with  $\tau$ , which is consistent with the qualitative discussion in Sec. II. Figure 9(a) shows good correspondence between the quantum and classical results for  $\tau < 9$ . For longer delays, the curves diverge. At the local maximum in Fig. 9(b) ( $\tau \approx 9$  ps), the enhanced (due to the prepulse) degree of orientation is an order of magnitude higher compared to the case of THz pulse alone. Figure 9(c) shows the global orientation maximum for various  $\tau$ . The dependence on  $\tau$  is periodic, and the period equal to half revival,  $T_{rev}/2 \approx 41.2$  ps. When  $\tau \approx T_{rev}/4$ , the maximum degree of orientation exhibits high-amplitude oscillations. The reason for this high sensitivity is the coalescence of the echo that appears *after* the THz pulse at  $t \approx 3\tau = 3T_{rev}/4$  and the echo that appears *before* the quantum revival at  $t \approx T_{rev} - \tau = 3T_{rev}/4$ . Notice, the orientation can be further enhanced using a stronger prepulse (see Fig. 5 in Sec. II).

Previously, related schemes for enhancing the THz- and two-color-induced orientation were applied to cold OCS molecules (at 2 K in [43], and at 25 K in [77]). The orientation was substantially enhanced with the help of an aligning laser pulse. The delay between the aligning and orienting pulses was set to  $T_{rev}/4$ . The authors explained the enhancements using quantum mechanical arguments.

### C. Results: symmetric-top molecule

To demonstrate the robustness of the proposed orientation enhancement mechanism, we consider an addition example molecule  $\text{CH}_3\text{I}$  that belongs to the class of symmetric-top molecules. The molecular properties were taken from NIST (DFT, method: CAM-B3LYP/cc-pVTZ-PP) [121]:  $I_x = I_y \equiv I = 68.527 \text{ amu } \text{\AA}^2$ ,  $I_z = 3.23 \text{ amu } \text{\AA}^2$ ,  $\mu = 1.697 \text{ Debye}$ , and  $\Delta\alpha = 2.951 \text{ \AA}^3$ .

Figure 10 shows the orientation factor obtained using the quantum simulation at room temperature. The delay between the pulses was set to  $\tau = 9$  ps [see Eq. (8)]. All the parameters are the same as in Fig. 8, except the lower peak amplitude of the THz pulse,  $\varepsilon_{0,THz} = 0.3 \text{ MV/cm}$ . On the short time scale, the quantum and classical results are close. The maximum orientation emerges before the quantum revival (during the quantum echo). The maxi-

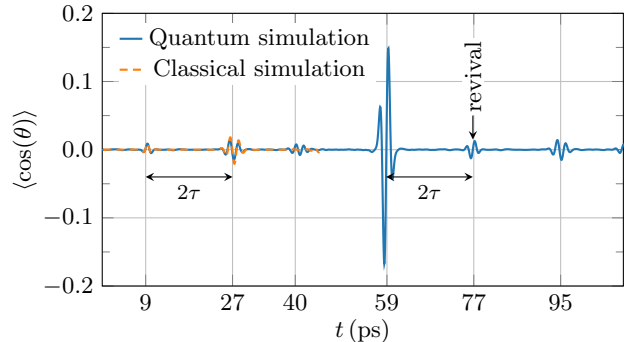


FIG. 10. Orientation factor for  $\text{CH}_3\text{I}$  molecules calculated quantum mechanically and classically at  $T = 300$  K. The delay between the stratifying and the THz pulses is  $\tau = 9$  ps. The field parameters are the same as in Fig. 8, except the THz field intensity  $\varepsilon_{0,THz} = 0.3 \text{ MV/cm}$ . The maximum orientation factor obtained using only the THz pulse is  $\approx 0.016$ .

imum orientation obtained using the THz pulse alone at room temperature is ten times lower,  $\approx 1.6\%$ .

## IV. CONCLUSION

In this work, we introduced an echo-based approach for enhancing the field-free molecular orientation induced by THz pulses at high temperatures. The enhancement mechanism relies on the general nonlinear phenomenon of phase space filamentation and requires a single additional non-resonant laser pulse before the orienting THz excitation. The intense laser pulse effectively eliminates the detrimental thermal broadening by producing multiple separated narrow filaments in the molecular rotational phase space. Molecular subgroups forming individual filaments are effectively cold and easy to orient. The overall significant orientation of the whole ensemble is achieved in the course of echoes forming at set time delays. The various echoes emerging from the combined laser and THz excitation are qualitatively explained using the transparent and intuitive 2D model. In particular, we show that of many echoes possible, the so-called quantum echo, gives rise to the especially pronounced orientation enhancement. In the examples presented in the paper, the maximum orientation at room temperature reaches  $\sim 20\%$ . With prepulses of higher intensity and various optimization procedures, even higher orientation can be expected. We demonstrate the robustness of the proposed scheme by using fully quantum simulations of the dynamics of linear (OCS) and symmetric-top ( $\text{CH}_3\text{I}$ ) molecules at room temperature. In principle, the temperature range over which the current methodology is operating is not limited to room temperature. Higher temperature regimes could be explored, which may help study materials with low vapor pressure. The high degree of orientation in a thermal gas paves the way to unprecedented imaging opportunities, chemical reaction control, and more.

## ACKNOWLEDGMENTS

L.X. is a recipient of the Sir Charles Clore Postdoctoral Fellowship. This research was made possible in part by the historic generosity of the Harold Perlman Family.

## Appendix A: Impulsive approximation

One of the tools for inducing molecular orientation is a half-cycle THz pulse [43]. The interaction of such a pulse with the permanent molecular dipole can be modeled using the potential

$$V_{or}(\theta, t) = -\mu\varepsilon_{or}(t) \cos(\theta), \quad (\text{A1})$$

where  $\mu$  is the molecular dipole moment magnitude,  $\varepsilon_{or}(t)$  defines the electric field's time dependence, and  $\theta$  is the polar angle between the molecular axis and the electric field vector. For the sake of the model, we assume that  $\varepsilon_{or}(t)$  is Gaussian

$$\varepsilon_{or}(t) = \varepsilon_{0,or} \exp[-t^2/\sigma_{or}^2], \quad (\text{A2})$$

where  $\varepsilon_{0,or}$  is the peak amplitude of the electric field,  $\sigma_{or}$  is the width of the pulse. The equation of motion for the molecular angular momentum  $L$  is

$$\frac{dL}{dt} = -\frac{dV_{or}(\theta)}{d\theta} = -\mu\varepsilon_{or}(t) \sin(\theta). \quad (\text{A3})$$

In the impulsive approximation, when the change in  $\theta$  is negligible during the pulse, the change in  $L$  due to the orienting interaction is

$$\Delta L_{or} = -\sqrt{\pi}\mu\sigma_{or}\varepsilon_{0,or} \sin(\theta_0), \quad (\text{A4})$$

where  $\theta_0$  is the angle at the moment of the pulse, and  $P_{or}$  is defined as

$$P_{or} = \frac{\mu\sqrt{\pi}}{I}\sigma_{or}\varepsilon_{0,or}, \quad (\text{A5})$$

where  $I$  is the molecule's moment of inertia.

A standard tool for inducing molecular alignment is non-resonant femtosecond laser pulses. We use such a pulse as a prepulse to stratify the phase space, see Sec. II. The interaction of a molecule with the prepulse is modeled as

$$V_{pre}(\theta, t) = -\frac{\Delta\alpha}{4}\varepsilon_{pre}^2(t) \cos^2(\theta), \quad (\text{A6})$$

where  $\Delta\alpha$  is the polarizability anisotropy of the molecule. The potential in Eq. (A6) is averaged over the laser's optical cycle. The function  $\varepsilon_{pre}(t)$  is the slowly varying Gaussian envelope of the laser pulse

$$\varepsilon_{pre}(t) = \varepsilon_{0,pre} \exp[-2\ln(2)t^2/\sigma_{pre}^2], \quad (\text{A7})$$

where  $\varepsilon_{0,pre}$  is the peak amplitude of the laser's electric field,  $\sigma_{pre}$  is the full width at half maximum of the laser pulse intensity. In the impulsive approximation

$$\Delta L_{pre} = -\sqrt{\frac{\pi}{\ln(16)}}\frac{\Delta\alpha}{4}\sigma_{pre}\varepsilon_{0,pre} \sin(2\theta_0), \quad (\text{A8})$$

and  $P_{pre}$  is defined as

$$P_{pre} = \sqrt{\frac{\pi}{\ln(16)}}\frac{\Delta\alpha}{4I}\sigma_{pre}\varepsilon_{0,pre}. \quad (\text{A9})$$

## Appendix B: Orientation factor

Here, we derive the formulas for the orientation factor

$$\langle \cos(\theta) \rangle (t) = \langle \text{Re}(e^{i\theta}) \rangle (t) = \text{Re}[\langle e^{i\theta} \rangle (t)], \quad (\text{B1})$$

where the angle brackets denote ensemble average, for two cases: (i) excitation by an orienting pulse alone, and (ii) excitation by a prepulse followed by an orienting kick.

## 1. Single orienting pulse

The time-dependent orientation factor after the orienting excitation is given by the real part of

$$\begin{aligned} \langle e^{i\theta} \rangle (t) &= (2\pi)^{-3/2}\sigma_T^{-1} \\ &\times \int_{-\infty}^{\infty} \int_0^{2\pi} \exp\{i[\theta_0 + \omega_0 t - P_{or} \sin(\theta_0)t]\} \\ &\times \exp[-\omega_0^2/(2\sigma_T^2)] d\theta_0 d\omega_0 \\ &= (2\pi)^{-3/2}\sigma_T^{-1} \int_{-\infty}^{\infty} e^{i\omega_0 t} \exp[-\omega_0^2/(2\sigma_T^2)] d\omega_0 \\ &\times \int_0^{2\pi} e^{i\theta_0} \exp[-iP_{or} \sin(\theta_0)t] d\theta_0, \end{aligned} \quad (\text{B2})$$

where  $\sigma_T = \sqrt{k_B T/I}$ , and  $\theta(t) = \theta_0 + \omega_0 t - P_{or} \sin(\theta_0)t$  [see Eq. (1)]. Using the Jacobi–Anger expansion

$$e^{iz \sin(\theta)} = \sum_{k=-\infty}^{\infty} e^{ik\theta} J_k(z), \quad (\text{B3})$$

where  $J_k(z)$  is the Bessel function of integer order  $k$ , we can represent the second integral in Eq. (B2) as

$$\begin{aligned} &\int_0^{2\pi} e^{i\theta_0} \exp[-iP_{or} \sin(\theta_0)t] d\theta_0 \\ &= \sum_{k=-\infty}^{\infty} \int_0^{2\pi} e^{i\theta_0} e^{-ik\theta_0} J_k(P_{or}t) d\theta_0 \\ &= 2\pi J_1(P_{or}t), \end{aligned} \quad (\text{B4})$$

where all the terms in the sum, except for  $k = 1$ , vanish. Finally,

$$\langle \cos(\theta) \rangle (t) = e^{-\sigma_T^2 t^2/2} J_1(P_{or}t). \quad (\text{B5})$$

## 2. Stratifying prepulse followed by orienting kick

Just after the stratifying kick (prepulse), the rotor's variables are

$$\begin{aligned} \theta_1(t) &= \theta_0 + \omega_1 t, \\ \omega_1 &= \omega_0 - P_{pre} \sin(2\theta_0), \end{aligned} \quad (\text{B6})$$

After a delay equal to  $\tau$ , at  $t = \tau$ , we apply the orienting kick after which the rotor's variables are

$$\begin{aligned} \theta_2(t) &= \theta_1(\tau) + (t - \tau)\omega_2, \\ \omega_2 &= \omega_1 - P_{or} \sin[\theta_1(\tau)]. \end{aligned} \quad (\text{B7})$$

The orientation factor is given by the real part of

$$\begin{aligned} \langle e^{i\theta} \rangle (t) &= \Theta(t - \tau) \frac{(2\pi)^{-3/2}}{\sigma_T} \int_{-\infty}^{\infty} \int_0^{2\pi} \exp[i\theta_2(t)] \\ &\times \exp[-\omega_0^2/(2\sigma_T^2)] d\theta_0 d\omega_0, \end{aligned} \quad (\text{B8})$$

where  $\Theta(t - \tau)$  is the step function. We use Eqs. (B6) and (B7) to express  $\theta_2$  in terms of  $\theta_0$  and  $\omega_0$ . Next, we use the Jacobi–Anger expansion

$$\begin{aligned} &\exp\{iP_{or}(t - \tau) \sin[-\theta_0 - \omega_0\tau + P_{pre} \sin(2\theta_0)\tau]\} \\ &= \sum_{k=-\infty}^{\infty} (\exp\{-ik[\theta_0 + \omega_0\tau - P_{pre} \sin(2\theta_0)\tau]\} \\ &\times J_k[P_{or}(t - \tau)]) \end{aligned} \quad (\text{B9})$$

Combining the terms proportional to  $\omega_0$  in the exponent, we get  $\exp[i\omega_0 t - ik\omega_0 \tau]$ . Integral  $d\omega_0$  then yields

$$\int_{-\infty}^{\infty} \exp[i\omega_0(t - k\tau)] e^{-\omega_0^2/(2\sigma_T^2)} d\omega_0 = \sqrt{2\pi}\sigma_T e^{-\sigma_T^2(t-k\tau)^2/2}. \quad (\text{B10})$$

The rest of the terms in the exponent read

$$\begin{aligned} & \exp[i\theta_0 - iP_{pre} \sin(2\theta_0)t - ik\theta_0 + ikP_{pre} \sin(2\theta_0)\tau] \\ &= \exp[i\theta_0(1 - k) + iP_{pre} \sin(2\theta_0)(k\tau - t)] \\ &= \sum_{m=-\infty}^{\infty} \exp[i\theta_0(1 - k + 2m)] J_m[P_{pre}(k\tau - t)]. \quad (\text{B11}) \end{aligned}$$

Integral  $d\theta_0$  then yields

$$\begin{aligned} & \int_0^{2\pi} \sum_{m=-\infty}^{\infty} \exp[i\theta_0(1 - k + 2m)] J_m[P_{pre}(k\tau - t)] d\theta_0 \\ &= 2\pi \sum_{m=-\infty}^{\infty} \delta(1 - k + 2m) J_m[P_{pre}(k\tau - t)] \\ &= \begin{cases} 2\pi J_{\frac{k-1}{2}}[P_{pre}(k\tau - t)], & \text{odd } k, \\ 0, & \text{even } k. \end{cases} \quad (\text{B12}) \end{aligned}$$

Overall, the orientation signal reads

$$\langle \cos(\theta) \rangle (t) = \Theta(t - \tau) \sum_{\text{odd } k}^{\infty} S_k(t), \quad (\text{B13})$$

where

$$\begin{aligned} S_k(t) &= e^{-\sigma_T^2(t-k\tau)^2/2} J_k[P_{or}(t - \tau)] \\ &\quad \times J_{\frac{k-1}{2}}[P_{pre}(k\tau - t)]. \quad (\text{B14}) \end{aligned}$$

### Appendix C: Quantum rigid rotor

The energy eigenstates of the quantum rotor restricted to the  $XY$  plane are  $\psi_n = \exp(i\phi n)/\sqrt{2\pi}$ , where  $n = 0, \pm 1, \pm 2, \dots$ . The energies (in atomic units,  $\hbar = 1$ ) are  $E_n = n^2/(2I)$ , where  $I$  is the moment of inertia. Like in the classical case, we treat the effect of the stratifying (prepulse) and orienting kicks in the impulsive approximation. The prepulse transforms an initial wave function  $\psi_-$  into  $\psi_+ = \exp[iIP_{pre} \cos^2(\theta)]\psi_-$ , where  $P_{pre}$  is given by Eq. (A9). Similarly, for the orienting kick  $\psi_+ = \exp[iIP_{or} \cos(\theta)]\psi_-$ , where  $P_{or}$  is given by (A5).

Each of the basis wave functions,  $\psi_n$  is ‘‘kicked’’ and propagated in time. The final observable, the ensemble averaged orientation factor,  $\langle \cos(\theta) \rangle$  is obtained by thermal averaging over the various expectation values  $\langle \Psi_n(\theta, t) | \cos(\theta) | \Psi_n(\theta, t) \rangle$ , where  $\Psi_n(\theta, t)$  is the wave function at time  $t$  corresponding to the initial state  $\psi_n$ .

- 
- [1] H. Stapelfeldt and T. Seideman, Colloquium: Aligning molecules with strong laser pulses, *Rev. Mod. Phys.* **75**, 543 (2003).
- [2] Y. Ohshima and H. Hasegawa, Coherent rotational excitation by intense nonresonant laser fields, *Int. Rev. Phys. Chem.* **29**, 619 (2010).
- [3] S. Fleischer, Y. Khodorkovsky, E. Gershnel, Y. Prior, and I. Sh. Averbukh, Molecular alignment induced by ultrashort laser pulses and its impact on molecular motion, *Isr. J. Chem.* **52**, 414 (2012).
- [4] M. Lemeshko, R. V. Krems, J. M. Doyle, and S. Kais, Manipulation of molecules with electromagnetic fields, *Mol. Phys.* **111**, 1648 (2013).
- [5] C. P. Koch, M. Lemeshko, and D. Sugny, Quantum control of molecular rotation, *Rev. Mod. Phys.* **91**, 035005 (2019).
- [6] K. Lin, I. Tutunnikov, J. Ma, J. Qiang, L. Zhou, O. Faucher, Y. Prior, I. Sh. Averbukh, and J. Wu, Spatiotemporal rotational dynamics of laser-driven molecules, *Adv. Photon.* **2**, 024002 (2020).
- [7] B. Friedrich and D. Herschbach, Enhanced orientation of polar molecules by combined electrostatic and nonresonant induced dipole forces, *J. Chem. Phys.* **111**, 6157 (1999).
- [8] B. Friedrich and Herschbach, Manipulating molecules via combined static and laser fields, *J. Phys. Chem. A* **103**, 10280 (1999).
- [9] H. Sakai, S. Minemoto, H. Nanjo, H. Tanji, and T. Suzuki, Controlling the orientation of polar molecules with combined electrostatic and pulsed, nonresonant laser fields, *Phys. Rev. Lett.* **90**, 083001 (2003).
- [10] A. Goban, S. Minemoto, and H. Sakai, Laser-field-free molecular orientation, *Phys. Rev. Lett.* **101**, 013001 (2008).
- [11] O. Ghafur, A. Rouzée, A. Gijsbertsen, W. K. Siu, S. Stolte, and M. J. J. Vrakking, Impulsive orientation and alignment of quantum-state-selected NO molecules, *Nat. Phys.* **5**, 289 (2009).
- [12] L. Holmegaard, J. H. Nielsen, I. Nevo, H. Stapelfeldt, F. Filsinger, J. Küpper, and G. Meijer, Laser-induced alignment and orientation of quantum-state-selected large molecules, *Phys. Rev. Lett.* **102**, 023001 (2009).
- [13] J. H. Mun, D. Takei, S. Minemoto, and H. Sakai, Laser-field-free orientation of state-selected asymmetric top molecules, *Phys. Rev. A* **89**, 051402(R) (2014).
- [14] D. Takei, J. H. Mun, S. Minemoto, and H. Sakai, Laser-field-free three-dimensional molecular orientation, *Phys. Rev. A* **94**, 013401 (2016).
- [15] J. J. Omiste and R. González-Férez, Theoretical description of the mixed-field orientation of asymmetric-top molecules: A time-dependent study, *Phys. Rev. A* **94**, 063408 (2016).
- [16] L. V. Thesing, J. Küpper, and R. González-Férez, Time-dependent analysis of the mixed-field orientation of molecules without rotational symmetry, *J. Chem. Phys.* **146**, 244304 (2017).
- [17] M. J. J. Vrakking and S. Stolte, Coherent control of molecular orientation, *Chem. Phys. Lett.* **271**, 209 (1997).
- [18] C. Dion, A. Bandrauk, O. Atabek, A. Keller, H. Umeda, and Y. Fujimura, Two-frequency IR laser orientation of polar molecules. numerical simulations for HCN, *Chem. Phys. Lett.* **302**, 215 (1999).
- [19] T. Kanai and H. Sakai, Numerical simulations of molecular orientation using strong, nonresonant, two-color laser fields, *J. Chem. Phys.* **115**, 5492 (2001).
- [20] N. Takemoto and K. Yamanouchi, Fixing chiral molecules in space by intense two-color phase-locked laser fields, *Chem. Phys. Lett.* **451**, 1 (2008).
- [21] S. De, I. Znakovskaya, D. Ray, F. Anis, N. G. Johnson,

- I. A. Bocharova, M. Magrakvelidze, B. D. Esry, C. L. Cocke, I. V. Litvinyuk, and M. F. Kling, Field-Free Orientation of CO Molecules by Femtosecond Two-Color Laser Fields, *Phys. Rev. Lett.* **103**, 153002 (2009).
- [22] K. Oda, M. Hita, S. Minemoto, and H. Sakai, All-optical molecular orientation, *Phys. Rev. Lett.* **104**, 213901 (2010).
- [23] J. Wu and H. Zeng, Field-free molecular orientation control by two ultrashort dual-color laser pulses, *Phys. Rev. A* **81**, 053401 (2010).
- [24] S. Zhang, J. Shi, H. Zhang, T. Jia, Z. Wang, and Z. Sun, Field-free molecular orientation by a multicolor laser field, *Phys. Rev. A* **83**, 023416 (2011).
- [25] E. Frumker, C. T. Hebeisen, N. Kajumba, J. B. Bertrand, H. J. Wörner, M. Spanner, D. M. Villeneuve, A. Naumov, and P. B. Corkum, Oriented rotational wave-packet dynamics studies via high harmonic generation, *Phys. Rev. Lett.* **109**, 113901 (2012).
- [26] M. Spanner, S. Patchkovskii, E. Frumker, and P. Corkum, Mechanisms of two-color laser-induced field-free molecular orientation, *Phys. Rev. Lett.* **109**, 113001 (2012).
- [27] I. Znakovskaya, M. Spanner, S. De, H. Li, D. Ray, P. Corkum, I. V. Litvinyuk, C. L. Cocke, and M. F. Kling, Transition between mechanisms of laser-induced field-free molecular orientation, *Phys. Rev. Lett.* **112**, 113005 (2014).
- [28] K. Lin, I. Tutunnikov, J. Qiang, J. Ma, Q. Song, Q. Ji, W. Zhang, H. Li, F. Sun, X. Gong, H. Li, P. Lu, H. Zeng, Y. Prior, I. Sh. Averbukh, and J. Wu, All-optical field-free three-dimensional orientation of asymmetric-top molecules, *Nat. Commun.* **9**, 5134 (2018).
- [29] D. Mellado-Alcedo, N. R. Quintero, and R. González-Férez, Linear polar molecule in a two-color cw laser field: A symmetry analysis, *Phys. Rev. A* **102**, 023110 (2020).
- [30] S. Wang and N. E. Henriksen, Optimal field-free molecular orientation with nonresonant two-color adiabatic-turn-on and sudden-turn-off laser pulses, *Phys. Rev. A* **102**, 063120 (2020).
- [31] L. Xu, I. Tutunnikov, Y. Prior, and I. Sh. Averbukh, Long-lasting orientation of symmetric-top molecules excited by two-color femtosecond pulses, *Front. Phys.* **9**, 689635 (2021).
- [32] A. Yachmenev and S. N. Yurchenko, Detecting chirality in molecules by linearly polarized laser fields, *Phys. Rev. Lett.* **117**, 033001 (2016).
- [33] E. Gershnel and I. Sh. Averbukh, Orienting asymmetric molecules by laser fields with twisted polarization, *Phys. Rev. Lett.* **120**, 083204 (2018).
- [34] I. Tutunnikov, E. Gershnel, S. Gold, and I. Sh. Averbukh, Selective orientation of chiral molecules by laser fields with twisted polarization, *J. Phys. Chem. Lett.* **9**, 1105 (2018).
- [35] A. A. Milner, J. A. M. Fordyce, I. MacPhail-Bartley, W. Wasserman, V. Milner, I. Tutunnikov, and I. Sh. Averbukh, Controlled Enantioselective Orientation of Chiral Molecules with an Optical Centrifuge, *Phys. Rev. Lett.* **122**, 223201 (2019).
- [36] I. Tutunnikov, J. Floß, E. Gershnel, P. Brumer, and I. Sh. Averbukh, Laser-induced persistent orientation of chiral molecules, *Phys. Rev. A* **100**, 043406 (2019).
- [37] I. Tutunnikov, J. Floß, E. Gershnel, P. Brumer, I. Sh. Averbukh, A. A. Milner, and V. Milner, Observation of persistent orientation of chiral molecules by a laser field with twisted polarization, *Phys. Rev. A* **101**, 021403(R) (2020).
- [38] L. Xu, Enantioselective chiral orientation induced by a combination of a long and a short laser pulse, *Phys. Rev. A* **105**, 033113 (2022).
- [39] H. Harde, S. Keiding, and D. Grischkowsky, THz commensurate echoes: Periodic rephasing of molecular transitions in free-induction decay, *Phys. Rev. Lett.* **66**, 1834 (1991).
- [40] M. Machholm and N. E. Henriksen, Field-free orientation of molecules, *Phys. Rev. Lett.* **87**, 193001 (2001).
- [41] S. Fleischer, Y. Zhou, R. W. Field, and K. A. Nelson, Molecular Orientation and Alignment by Intense Single-Cycle THz Pulses, *Phys. Rev. Lett.* **107**, 163603 (2011).
- [42] K. Kitano, N. Ishii, N. Kanda, Y. Matsumoto, T. Kanai, M. Kuwata-Gonokami, and J. Itatani, Orientation of jet-cooled polar molecules with an intense single-cycle THz pulse, *Phys. Rev. A* **88**, 061405(R) (2013).
- [43] K. N. Egodapitiya, S. Li, and R. R. Jones, Terahertz-induced field-free orientation of rotationally excited molecules, *Phys. Rev. Lett.* **112**, 103002 (2014).
- [44] R. Damari, S. Kallush, and S. Fleischer, Rotational control of asymmetric molecules: Dipole- versus polarizability-driven rotational dynamics, *Phys. Rev. Lett.* **117**, 103001 (2016).
- [45] P. Babilotte, K. Hamraoui, F. Billard, E. Hertz, B. Lavorel, O. Faucher, and D. Sugny, Observation of the field-free orientation of a symmetric-top molecule by terahertz laser pulses at high temperature, *Phys. Rev. A* **94**, 043403 (2016).
- [46] P. Babilotte, L. H. Coudert, F. Billard, E. Hertz, O. Faucher, and B. Lavorel, Experimental and theoretical study of free induction decay of water molecules induced by terahertz laser pulses, *Phys. Rev. A* **95**, 043408 (2017).
- [47] L. Xu, I. Tutunnikov, E. Gershnel, Y. Prior, and I. Sh. Averbukh, Long-lasting molecular orientation induced by a single terahertz pulse, *Phys. Rev. Lett.* **125**, 013201 (2020).
- [48] I. Tutunnikov, L. Xu, R. W. Field, K. A. Nelson, Y. Prior, and I. Sh. Averbukh, Enantioselective orientation of chiral molecules induced by terahertz pulses with twisted polarization, *Phys. Rev. Res.* **3**, 013249 (2021).
- [49] A. Beer, R. Damari, Y. Chen, and S. Fleischer, Molecular Orientation-Induced Second-Harmonic Generation: Deciphering Different Contributions Apart, *J. Phys. Chem. A* **126**, 3732 (2022).
- [50] I. Sh. Averbukh and R. Arvieu, Angular focusing, squeezing, and rainbow formation in a strongly driven quantum rotor, *Phys. Rev. Lett.* **87**, 163601 (2001).
- [51] M. Leibscher, I. Sh. Averbukh, and H. Rabitz, Molecular alignment by trains of short laser pulses, *Phys. Rev. Lett.* **90**, 213001 (2003).
- [52] M. Leibscher, I. Sh. Averbukh, and H. Rabitz, Enhanced molecular alignment by short laser pulses, *Phys. Rev. A* **69**, 013402 (2004).
- [53] S. Zhang, C. Lu, T. Jia, Z. Wang, and Z. Sun, Field-free molecular orientation enhanced by two dual-color laser subpulses, *J. Chem. Phys.* **135**, 034301 (2011).
- [54] X.-M. Zhang, J. Li, J. Yu, and S.-L. Cong, Field-Free Molecular Orientation Induced by a Single-Cycle THz Laser Pulse Train, *Commun. Comput. Phys.* **20**, 689 (2016).
- [55] K. Nakajima, H. Abe, and Y. Ohtsuki, Optimal control simulation of field-free molecular orientation: Alignment-enhanced molecular orientation, *J. Phys. Chem. A* **116**, 11219 (2012).
- [56] J. H. Mun and H. Sakai, Improving molecular orientation by optimizing relative delay and intensities of two-color laser pulses, *Phys. Rev. A* **98**, 013404 (2018).
- [57] J. H. Mun, H. Sakai, and R. González-Férez, Orientation of linear molecules in two-color laser fields with perpendicularly crossed polarizations, *Phys. Rev. A* **99**, 053424 (2019).
- [58] J. H. Mun and D. E. Kim, Field-free molecular orientation by delay- and polarization-optimized two fs pulses, *Sci. Rep.* **10**, 18875 (2020).
- [59] Md. Maruf Hossain and H. Sakai, All-optical orientation of linear molecules with combined linearly and elliptically polarized two-color laser fields, *J. Chem. Phys.*

- [153](#), [104102](#) (2020).
- [60] X.-F. Yu and S. Wang, Molecular orientation of thermal ensemble induced by two-color slow turn-on and rapid turn-off laser pulses, *Chem. Phys. Lett.* **784**, 139085 (2021).
- [61] Md. Maruf Hossain, X. Zhang, S. Minemoto, and H. Sakai, Stronger orientation of state-selected OCS molecules with relative-delay-adjusted nanosecond two-color laser pulses, *J. Chem. Phys.* **156**, 041101 (2022).
- [62] S. Wang and N. E. Henriksen, Optimal field-free molecular orientation with nonresonant two-color adiabatic-turn-on and sudden-turn-off laser pulses, *Phys. Rev. A* **102**, 063120 (2020).
- [63] M. Zhou, L.-H. Li, J. Yu, and S.-L. Cong, Field-free molecular orientation induced by a four-color laser pulse, *Chem. Phys.* **544**, 111114 (2021).
- [64] L. Xu, I. Tutunnikov, Y. Prior, and I. Sh. Averbukh, [Optimal selective orientation of chiral molecules using femtosecond laser pulses](#) (2022).
- [65] M. Spanner, E. A. Shapiro, and M. Ivanov, Coherent control of rotational wave-packet dynamics via fractional revivals, *Phys. Rev. Lett.* **92**, 093001 (2004).
- [66] D. Daems, S. Guérin, D. Sugny, and H. R. Jauslin, Efficient and long-lived field-free orientation of molecules by a single hybrid short pulse, *Phys. Rev. Lett.* **94**, 153003 (2005).
- [67] E. Gershnel, I. Sh. Averbukh, and R. J. Gordon, Orientation of molecules via laser-induced antialignment, *Phys. Rev. A* **73**, 061401(R) (2006).
- [68] E. Gershnel, I. Sh. Averbukh, and R. J. Gordon, Enhanced molecular orientation induced by molecular antialignment, *Phys. Rev. A* **74**, 053414 (2006).
- [69] K. Kitano, N. Ishii, and J. Itatani, High degree of molecular orientation by a combination of THz and femtosecond laser pulses, *Phys. Rev. A* **84**, 053408 (2011).
- [70] S. Zhang, C. Lu, T. Jia, Z. Wang, and Z. Sun, Controlling field-free molecular orientation with combined single- and dual-color laser pulses, *Phys. Rev. A* **83**, 043410 (2011).
- [71] R. Tehini, M. Z. Hoque, O. Faucher, and D. Sugny, Field-free molecular orientation of  $^1\Sigma$  and  $^2\Pi$  molecules at high temperature, *Phys. Rev. A* **85**, 043423 (2012).
- [72] C.-C. Shu and N. E. Henriksen, Field-free molecular orientation induced by single-cycle THz pulses: The role of resonance and quantum interference, *Phys. Rev. A* **87**, 013408 (2013).
- [73] Y. Liu, J. Li, J. Yu, and S.-L. Cong, Field-free molecular orientation by two-color shaped laser pulse together with time-delayed THz laser pulse, *Laser Phys. Lett.* **10**, 076001 (2013).
- [74] H.-C. Tao, S. Wang, W.-S. Zhan, C. Hao, and H.-F. Li, Field-free orientation of CO molecule by combining two-color femtosecond laser pulse with time-delayed positively chirped laser pulse, *Eur. Phys. J. D* **72**, 141 (2018).
- [75] C. Z. Bisgaard, M. D. Poulsen, E. Péronne, S. S. Viftrup, and H. Stapelfeldt, Observation of enhanced field-free molecular alignment by two laser pulses, *Phys. Rev. Lett.* **92**, 173004 (2004).
- [76] D. Pinkham, K. E. Mooney, and R. R. Jones, Optimizing dynamic alignment in room temperature CO, *Phys. Rev. A* **75**, 013422 (2007).
- [77] K. Sonoda, A. Iwasaki, K. Yamanouchi, and H. Hasegawa, Field-free molecular orientation of nonadiabatically aligned OCS, *Chem. Phys. Lett.* **693**, 114 (2018).
- [78] E. L. Hahn, Spin Echoes, *Phys. Rev.* **80**, 580 (1950).
- [79] E. L. Hahn, Free nuclear induction, *Phys. Today* **6**, 4 (1953).
- [80] N. A. Kurnit, I. D. Abella, and S. R. Hartmann, Observation of a Photon Echo, *Phys. Rev. Lett.* **13**, 567 (1964).
- [81] S. Mukamel, *Principles of nonlinear optical spectroscopy* (Oxford University Press, New York, 1995).
- [82] F. Mezei, Neutron spin echo: A new concept in polarized thermal neutron techniques, *Z. Physik* **255**, 146 (1972).
- [83] R. M. Hill and D. E. Kaplan, Cyclotron Resonance Echo, *Phys. Rev. Lett.* **14**, 1062 (1965).
- [84] R. W. Gould, T. M. O'Neil, and J. H. Malmberg, Plasma Wave Echo, *Phys. Rev. Lett.* **19**, 219 (1967).
- [85] A. Bulatov, A. Kuklov, B. E. Vugmeister, and H. Rabitz, Echo in optical lattices: Stimulated revival of breathing oscillations, *Phys. Rev. A* **57**, 3788 (1998).
- [86] F. B. J. Buchkremer, R. Dumke, H. Levsen, G. Birkl, and W. Ertmer, Wave Packet Echoes in the Motion of Trapped Atoms, *Phys. Rev. Lett.* **85**, 3121 (2000).
- [87] M. Herrera, T. M. Antonsen, E. Ott, and S. Fishman, Echoes and revival echoes in systems of anharmonically confined atoms, *Phys. Rev. A* **86**, 023613 (2012).
- [88] G. Stupakov, Echo effect in hadron colliders, Technical Report, SSCL-579 [10.2172/7237216](#) (1992).
- [89] L. K. Spentzouris, J.-F. Ostiguy, and P. L. Colestock, Direct Measurement of Diffusion Rates in High Energy Synchrotrons Using Longitudinal Beam Echoes, *Phys. Rev. Lett.* **76**, 620 (1996).
- [90] G. Stupakov, *Handbook of Accelerator Physics and Engineering*, 2nd ed., edited by A. W. Chau et. al (World Scientific, 2013) Chap. 2.3.13, pp. 121–123.
- [91] T. Sen and Y. S. Li, Nonlinear theory of transverse beam echoes, *Phys. Rev. Accel. Beams* **21**, 021002 (2018).
- [92] E. Hemsing, G. Stupakov, D. Xiang, and A. Zholents, Beam by design: Laser manipulation of electrons in modern accelerators, *Rev. Mod. Phys.* **86**, 897 (2014).
- [93] I. Tutunnikov, K. V. Rajitha, and I. Sh. Averbukh, Echoes in a single quantum Kerr-nonlinear oscillator, *Phys. Rev. A* **103**, 013717 (2021).
- [94] I. Tutunnikov, K. V. Rajitha, A. Y. Voronin, V. V. Nesvizhevsky, and I. Sh. Averbukh, Impulsively excited gravitational quantum states: Echoes and time-resolved spectroscopy, *Phys. Rev. Lett.* **126**, 170403 (2021).
- [95] G. Morigi, E. Solano, B.-G. Englert, and H. Walther, Measuring irreversible dynamics of a quantum harmonic oscillator, *Phys. Rev. A* **65**, 040102 (2002).
- [96] T. Meunier, S. Gleyzes, P. Maioli, A. Auffeves, G. Nogues, M. Brune, J. M. Raimond, and S. Haroche, Rabi Oscillations Revival Induced by Time Reversal: A Test of Mesoscopic Quantum Coherence, *Phys. Rev. Lett.* **94**, 010401 (2005).
- [97] J. Qiang, I. Tutunnikov, P. Lu, K. Lin, W. Zhang, F. Sun, Y. Silberberg, Y. Prior, I. Sh. Averbukh, and J. Wu, Echo in a single vibrationally excited molecule, *Nat. Phys.* **16**, 328 (2020).
- [98] G. Karras, E. Hertz, F. Billard, B. Lavorel, J.-M. Hartmann, O. Faucher, E. Gershnel, Y. Prior, and I. Sh. Averbukh, Orientation and alignment echoes, *Phys. Rev. Lett.* **114**, 153601 (2015).
- [99] G. Karras, E. Hertz, F. Billard, B. Lavorel, G. Siour, J.-M. Hartmann, O. Faucher, E. Gershnel, Y. Prior, and I. Sh. Averbukh, Experimental observation of fractional echoes, *Phys. Rev. A* **94**, 033404 (2016).
- [100] K. Lin, P. Lu, J. Ma, X. Gong, Q. Song, Q. Ji, W. Zhang, H. Zeng, J. Wu, G. Karras, G. Siour, J.-M. Hartmann, O. Faucher, E. Gershnel, Y. Prior, and I. Sh. Averbukh, Echoes in Space and Time, *Phys. Rev. X* **6**, 041056 (2016).
- [101] K. Lin, J. Ma, X. Gong, Q. Song, Q. Ji, W. Zhang, H. Li, P. Lu, H. Li, H. Zeng, J. Wu, J.-M. Hartmann, O. Faucher, E. Gershnel, Y. Prior, and I. Sh. Averbukh, Rotated echoes of molecular alignment: fractional, high order and imaginary, *Opt. Express* **25**, 24917 (2017).
- [102] D. Rosenberg, R. Damari, and S. Fleischer, Echo spectroscopy in multilevel quantum-mechanical rotors, *Phys. Rev. Lett.* **121**, 234101 (2018).

- [103] H. Zhang, B. Lavorel, F. Billard, J.-M. Hartmann, E. Hertz, O. Faucher, J. Ma, J. Wu, E. Gershnel, Y. Prior, and I. Sh. Averbukh, Rotational echoes as a tool for investigating ultrafast collisional dynamics of molecules, *Phys. Rev. Lett.* **122**, 193401 (2019).
- [104] J. Ma, H. Zhang, B. Lavorel, F. Billard, E. Hertz, J. Wu, C. Boulet, J.-M. Hartmann, and O. Faucher, Observing collisions beyond the secular approximation limit, *Nat. Commun.* **10**, 5780 (2019).
- [105] J.-M. Hartmann, J. Ma, T. Delahaye, F. Billard, E. Hertz, J. Wu, B. Lavorel, C. Boulet, and O. Faucher, Molecular alignment echoes probing collision-induced rotational-speed changes, *Phys. Rev. Research* **2**, 023247 (2020).
- [106] J. Ma, H. Zhang, B. Lavorel, F. Billard, J. Wu, C. Boulet, J.-M. Hartmann, and O. Faucher, Ultrafast collisional dissipation of symmetric-top molecules probed by rotational alignment echoes, *Phys. Rev. A* **101**, 043417 (2020).
- [107] L. Xu, I. Tutunnikov, L. Zhou, K. Lin, J. Qiang, P. Lu, Y. Prior, I. Sh. Averbukh, and J. Wu, Echoes in unidirectionally rotating molecules, *Phys. Rev. A* **102**, 043116 (2020).
- [108] J. Ma, L. H. Coudert, F. Billard, M. Bournazel, B. Lavorel, J. Wu, G. Maroulis, J.-M. Hartmann, and O. Faucher, Echo-assisted impulsive alignment of room-temperature acetone molecules, *Phys. Rev. Research* **3**, 023192 (2021).
- [109] D. Lynden-Bell, Statistical Mechanics of Violent Relaxation in Stellar Systems, *Mon. Not. R. Astron. Soc.* **136**, 101 (1967).
- [110] G. Guignard, Phase space dynamics, in *Frontiers of Particle Beams*, edited by M. Month and S. Turner (Springer Berlin Heidelberg, Berlin, Heidelberg, 1988) pp. 1–50.
- [111] D. Xiang and G. Stupakov, Echo-enabled harmonic generation free electron laser, *Phys. Rev. ST Accel. Beams* **12**, 030702 (2009).
- [112] I. Sh. Averbukh and N. F. Perelman, Fractional revivals: Universality in the long-term evolution of quantum wave packets beyond the correspondence principle dynamics, *Phys. Lett. A* **139**, 449 (1989).
- [113] R. W. Robinett, Quantum wave packet revivals, *Phys. Rep* **392**, 1 (2004).
- [114] H. Goldstein, C. Poole, and J. Safko, *Classical Mechanics* (Addison Wesley, San Francisco, CA, 2002).
- [115] J. B. Kuipers, *Quaternions and Rotation Sequences: A Primer with Applications to Orbits, Aerospace and Virtual Reality* (Princeton University Press, Princeton, N.J., 1999).
- [116] E. A. Coutsiaris and L. Romero, The quaternions with an application to rigid body dynamics, Sandia Technical Report, SAND2004-0153 (2004).
- [117] R. V. Krems, *Molecules in Electromagnetic Fields: From Ultracold Physics to Controlled Chemistry* (Wiley, 2018).
- [118] R. B. Sidje, Expokit: A software package for computing matrix exponentials, *ACM Trans. Math. Softw.* **24**, 130 (1998).
- [119] S. Kallush and S. Fleischer, Orientation dynamics of asymmetric rotors using random phase wave functions, *Phys. Rev. A* **91**, 063420 (2015).
- [120] R. S. McDowell, Rotational partition functions for symmetric-top molecules, *J. Chem. Phys.* **93**, 2801 (1990).
- [121] R. D. Johnson, *NIST Computational chemistry comparison and benchmark database, Release 20*, Tech. Rep. (2019).
- [122] M. Clerici, M. Peccianti, B. E. Schmidt, L. Caspani, M. Shalaby, M. Giguère, A. Lotti, A. Couairon, F. Légaré, T. Ozaki, D. Faccio, and R. Morandotti, Wavelength Scaling of Terahertz Generation by Gas Ionization, *Phys. Rev. Lett.* **110**, 253901 (2013).
- [123] T. I. Oh, Y. J. Yoo, Y. S. You, and K. Y. Kim, Generation of strong terahertz fields exceeding 8 MV/cm at 1 kHz and real-time beam profiling, *Appl. Phys. Lett.* **105**, 041103 (2014).
- [124] C. Vicario, A. V. Ovchinnikov, S. I. Ashitkov, M. B. Agranat, V. E. Fortov, and C. P. Hauri, Generation of 0.9-mJ THz pulses in DSTMS pumped by a Cr:Mg<sub>2</sub>SiO<sub>4</sub> laser, *Opt. Lett.* **39**, 6632 (2014).
- [125] M. Shalaby and C. P. Hauri, Demonstration of a low-frequency three-dimensional terahertz bullet with extreme brightness, *Nat. Commun.* **6**, 5976 (2015).
- [126] M. Lapert and D. Sugny, Field-free molecular orientation by terahertz laser pulses at high temperature, *Phys. Rev. A* **85**, 063418 (2012).